ACS Catalysis

pubs.acs.org/acscatalysis

Research Article

Reversible Deactivation of Manganese Catalysts in Alkene Oxidation and H_2O_2 Disproportionation

Johann B. Kasper, Laia Vicens, C. Maurits de Roo, Ronald Hage, Miquel Costas,* and Wesley R. Browne*

Cite This: *ACS Catal.* 2023, 13, 6403−6415

Read Online

ACCESS | Metrics & More | Article Recommendations | Supporting Information

ABSTRACT: Mononuclear Mn^{II} oxidation catalysts with aminopyridine-based ligands achieve high turnover-number (TON) enantioselective epoxidation of alkenes with H_2O_2. Structure reactivity relations indicate a dependence of enantioselectivity and maximum TON on the electronic effect of peripheral ligand substituents. Competing H_2O_2 disproportionation is reduced by carrying out reactions at low temperatures and with slow addition of H_2O_2, which improve TONs for alkene oxidation but mask the effect of substituents on turnover frequency (TOF). Here, in situ Raman spectroscopy provides the high time resolution needed to establish that the minimum TOFs are greater than 10 s^{-1} in the epoxidation of alkenes with the complexes $[Mn(OTf)_2(^{R}PDP)]$ [where R = H (**^{H}PDP-Mn**) and R = OMe (**^{MeO}PDP-Mn**) and ^{R}PDP = *N*,*N*′-bis(2″-(4″-R-pyridylmethyl)-2,2′-bipyrrolidine)]. Simultaneous headspace monitoring by Raman spectroscopy reveals that H_2O_2 disproportionation proceeds concomitant with oxidation of the substrate and that the ratio of reactivity toward substrate oxidation and H_2O_2 disproportionation is ligand-dependent. Notably, the rates of substrate oxidation and H_2O_2 disproportionation both decrease over time under continuous addition of H_2O_2 due to progressive catalyst deactivation, which indicates that the same catalyst is responsible for both reactions. Electrochemistry, UV/vis absorption, and resonance Raman spectroscopy and spectroelectrochemistry establish that the Mn^{II} complexes undergo an increase in oxidation state within seconds of addition of H_2O_2 to form a dynamic mixture of Mn^{III} and Mn^{IV} species, with the composition depending on temperature and the presence of alkene. However, it is the formation of these complexes (resting states), rather than ligand degradation, that is responsible for catalyst deactivation, especially at low temperatures, and hence, the intrinsic reactivity of the catalyst is greater than observed TOFs. These data show that interpretation of effects of ligand substituents on reaction efficiency (and conversion) with respect to the oxidant and maximum TONs needs to consider reversible deactivation of the catalyst and especially the relative importance of various reaction pathways.

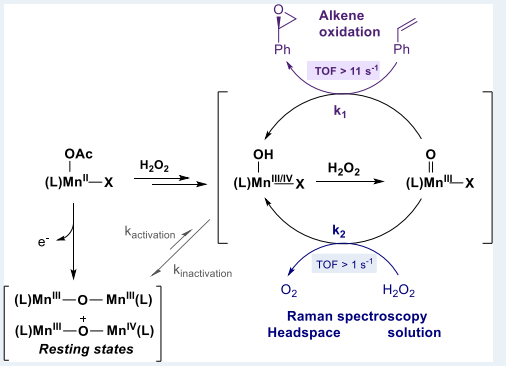

KEYWORDS: *manganese, epoxidation, Raman spectroscopy, mechanism, headspace analysis, alkene, disproportionation*

INTRODUCTION

The drive toward sustainable chemistry and, in particular, increasing atom economy of reactions has focused attention on catalytic methods using nonscarce elements.[1,2] Enantioselective oxidations of organic compounds focus increasingly on nonscarce/-toxic transition-metal-based catalysts, with oxidants such as H_2O_2 that give water as the only byproduct.[3,4] Manganese-based catalysts especially show excellent activity in the oxidation of wide range of organic substrates,[5,6] and manganese−salen complexes were shown by Jacobsen, Katsuki, and coworkers already in 1990 to provide good selectivity in alkene oxidations, including enantioselective epoxidations.[7−10] Over the last decades, amine ligand-based complexes have been developed with remarkable advances in turnover frequency and number (TOF and TON) and improved (enantio)selectivity.[11,12] In 2003, Stack and coworkers demonstrated that complexes of pyridyl-amine-based ligands, such as $[Mn^{II}(OTf)_2(MCP)]$ [MCP = *N*,*N*′-dimethyl-*N*,*N*′-bis(2-pyridylmethyl)cyclohexane-*trans*-1,2-diamine] (Scheme 1), catalyzed alkene epoxidations with high yields and TONs with peracetic acid as the terminal oxidant.[13,14] Attention to N-donor ligands increased subsequently with the groups of Bryliakov,[15−17] Sun,[18,19] and Costas,[20] reporting the reactivity of a wide range of variants of this class of catalysts for both epoxidation and C−H oxidation. In initial reports, peracetic acid was used as the terminal oxidant, but shortly thereafter, conditions with H_2O_2 as the terminal oxidant were developed,[21−23] although a large excess of carboxylic acid (up to 2000 equiv wrt catalyst) was required to achieve the

Received: February 23, 2023
Revised: April 8, 2023
Published: April 25, 2023

Scheme 1. Structures of Complexes Discussed in the Text and Typical Conditions for the Oxidation of Styrene with H_2O_2

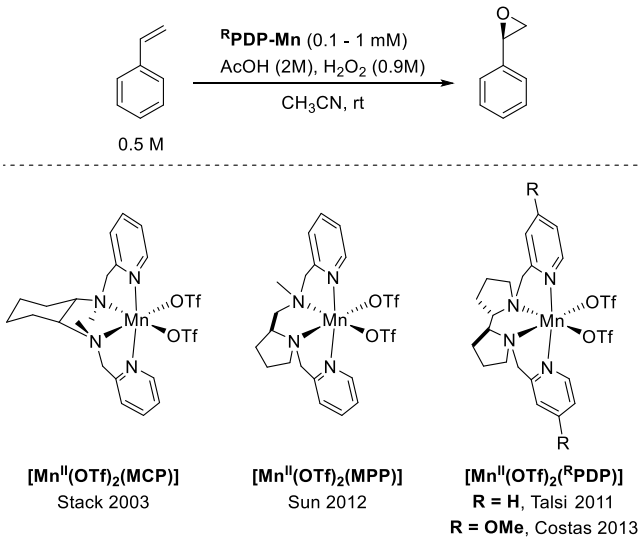

same performance reached with peracetic acid.[24] Elaboration of the catalyst and carboxylic acid cocatalyst and optimization of reaction conditions, e.g., catalyst and carboxylic acid concentration, temperature, etc., have led to high yields and enantioselectivities. In particular, sterically encumbered carboxylic acids provide the highest enantioselectivities in epoxidation, hinting at a role as ligands in the active catalytic species,[23] and supramolecular interactions can increase the effective (local) concentration of acid at the catalyst requiring only a few equivalents with respect to the catalyst.[25] These latter observations also indicate that carboxylic acids act as coligands to the catalyst.

The synthetic accessibility of the pyridyl amine class of ligands has facilitated variation in the structure of the ligands over the last decade, most notably with the aim to improve enantioselectivity and substrate scope.[11,12,26] Electron-donating groups at the para position of the pyridyl moiety generally improve enantioselectivity despite negligible steric influence (Scheme 1),[27,28] suggesting that they modify the electrophilicity and reactivity of a putative Mn^{V}=O species. ^{18}O-labeling studies, kinetic isotope effects, radical clocks, and Hammett analyses support this assignment.[28−34]

The structure−activity relations, established for substituents on the pyridyl moieties, indicate that they have a substantial impact on TONs achieved;[27,28] however, the conditions employed (continuous addition of oxidant) raise the question as to whether these differences are due to effects on intrinsic reactivity (TOF) or the catalysts' tendency toward deactivation. In the oxidation of alkenes with H_2O_2, typically, batchwise addition of the oxidant at subambient temperatures is employed with these catalysts to limit side reactions such as H_2O_2 disproportionation to H_2O and O_2. The efficiency (based on the amount of H_2O_2 employed vs the amount of the substrate converted) is dependent on the substrate and ranges from 50 to 80%, indicating that H_2O_2 decomposition is a significant aspect of the reactivity of the complexes.[15]

Here, we use in-line monitoring of both the reaction mixture and the headspace, under dropwise addition conditions, to determine the rate of oxidation of alkenes and competition from disproportionation to H_2O and O_2 by two mononuclear $[Mn^{II}(OTf)_2(^{R}PDP)]$ complexes [where R = H in **^{H}PDP-Mn**, R = OMe in **^{MeO}PDP-Mn**, and ^{R}PDP = *N*,*N*′-bis(2″-(4″-R-pyridylmethyl)-2,2′-bipyrrolidine), Scheme 1]. The choice of **^{H}PDP-Mn** and **^{MeO}PDP-Mn** for comparison is motivated by the differences in enantioselectivity, as well as TON reported for these complexes earlier.[27] We show that the reactions initially proceed with unusually high TOFs (>10 s^{-1}) for alkene oxidation, which then decrease over the course of dropwise addition of H_2O_2. Headspace monitoring shows that O_2 evolution is concomitant with alkene oxidation, indicating competing reaction pathways, in which the same catalyst is responsible for both alkene oxidation and H_2O_2 disproportionation. UV/vis absorption, resonance Raman, and electron paramagnetic resonance (EPR) spectroscopy are used to identify species formed under reaction conditions and establish their relevance to the catalytic cycle, as well as catalyst deactivation. The data indicate that the effect of substituents is not singular and can impact selectivity between alkene oxidation and unproductive H_2O_2 disproportionation (Scheme 2) and TOFs, as well as in the rate and extent of catalyst deactivation observed, which affects final TONs also.

Scheme 2. Initial Oxidation of Mn^{II} Catalysts by H_2O_2 in the Presence of Acetic Acid and Interconnected Reaction Pathways

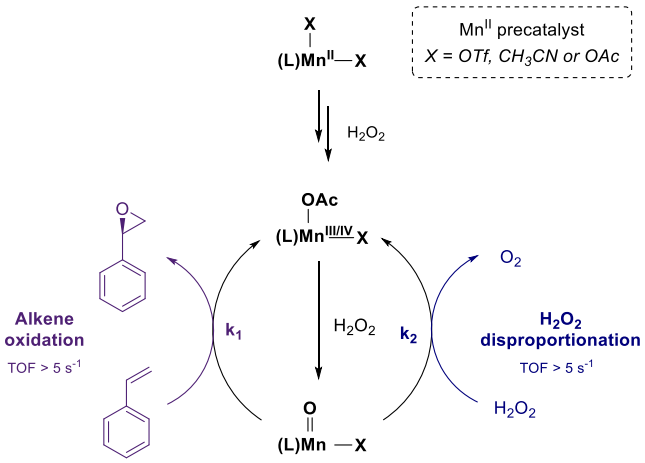

EXPERIMENTAL SECTION

Materials. Solvents and reagents were obtained from commercial sources and used as received unless stated otherwise. The complexes **^{H}PDP-Mn** and **^{MeO}PDP-Mn** were available from earlier studies and are enantiomerically pure.[16,27]

Methods. Fourier transform infrared (FTIR) spectra were recorded using a JASCO 4600 FTIR spectrometer equipped with a (PIKE) ATR unit. EPR spectra were recorded at 77 K in a finger dewar on an EMX Nano X-band EPR spectrometer (9.467 GHz, Bruker). Samples were held in capillaries and frozen rapidly by immersion in liquid nitrogen. Cyclic voltammetry was performed using a CHI760c bipotentiostat (CHInstruments) in a three-electrode arrangement with a Teflon-shrouded glassy carbon disc (3 mm diameter) working electrode, platinum wire counter electrode, and saturated calomel electrode (SCE) reference electrode in acetonitrile with 0.1 M KPF_6. UV/vis absorption spectroelectrochemistry was carried out with bulk electrolysis in a 2 mm pathlength

https://doi.org/10.1021/acscatal.3c00866
ACS Catal. 2023, 13, 6403−6415

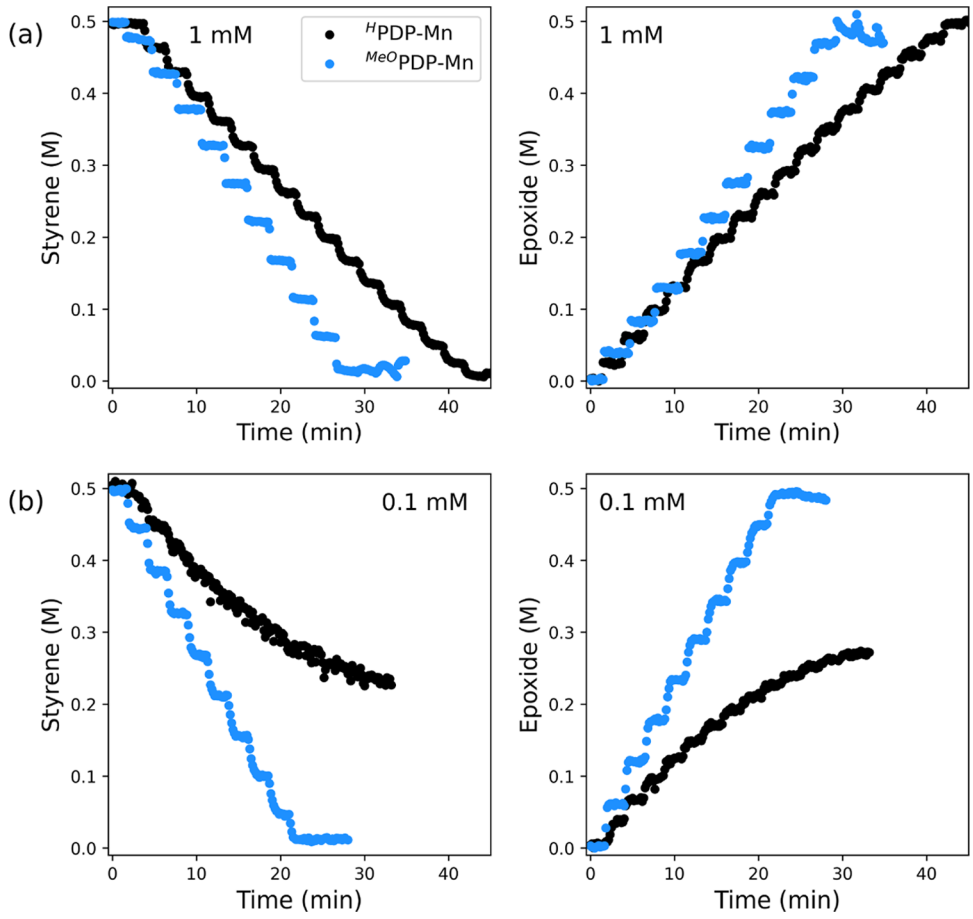

Figure 1. Concentrations of styrene and styrene epoxide over time with (a) 1 and (b) 0.1 mM catalyst (black—**^{H}PDP-Mn** and blue—**^{MeO}PDP-Mn**), 2 M AcOH, 0.135 equiv H_2O_2 drop^{-1} (average: 0.06 equiv H_2O_2 min^{-1}), monitored by Raman spectroscopy at 785 nm at 20 °C. Raman spectra before and after oxidation of styrene to styrene oxide; see Figure S2.

cuvette equipped with a platinum gauze (2 cm^2) working electrode, platinum wire counter electrode, and Ag/AgCl reference electrode. UV/vis absorption spectra were recorded on a Specord600 UV/vis absorption spectrometer (AnalytikJena). Raman spectra at 785 nm were recorded with a 500 mW fiber-coupled laser (Ondax), Raman probe (Inphotonics), and a Shamrock163i spectrograph equipped with an iVac-324FI CCD (Andor Technology) and 235 l/mm blazed at 750 nm. Raman spectra at 355 nm were recorded with a 10 mW laser at 355 nm (Cobolt Zouk) in a 180° backscattering configuration. A 7.5 cm focal length lens was used to focus the laser and collect and collimate Raman scattering. A long pass filter was used to reject Rayleigh scattering, and 15 cm focal length lens collected the Raman scattering into a Shamrock500 spectrograph with an 1800 l/mm grating blazed at 400 nm and an iDUS-420-BU2 CCD (Andor Technology). Spectra were acquired with Andor SOLIS and processed with SpectragrypH-On (F. Menges, version 1.2.14). Measurements at low temperature were recorded using either a Flash 300 temperature control cell (QNW) or a Unisoku USP-203 temperature control cell.

Reaction Progress Monitoring with Raman and UV/Vis Absorption Spectroscopy. Stock solutions of the catalysts were prepared in CH_3CN [5 mM, 3.38 mg of (**^{H}PDP-Mn**) or 3.69 mg of (**^{MeO}PDP-Mn**) in 1 mL of CH_3CN]. Reaction mixtures (1.5 mL total volume) were prepared with styrene (0.5 M, 86 μL), AcOH (2 M, 172 μL), and catalyst (0.1−1 mM, 30−300 μL from stock solution) in CH_3CN. H_2O_2 [from a 50% (w/w) solution in H_2O] was added in a preprepared 1:1 (v/v) solution in CH_3CN. The oxidant solution was added by a syringe pump at a flow rate of 5.1 μL min^{-1}. The average time between drops falling into the solution was 135 s (0.135 equiv H_2O_2 per drop). The solutions remained homogeneous throughout the reaction. Raman spectra (λ_{exc} 785 nm) and UV/vis absorption spectra were recorded simultaneously before and during the addition of H_2O_2. Raman spectra of the neat compounds and the analysis of the Raman data are described in the Supporting Information (Figures S1 and S2, respectively). For some experiments, UV/vis absorption spectroscopy with the addition of a few equivalents of H_2O_2 to a reaction mixture as prepared for catalysis was performed with manual addition of a dilute solution H_2O_2 in CH_3CN for greater control in regard to the number of equivalents with respect to the catalyst. Headspace analysis of reactions was carried out with simultaneous use of two Raman probes (λ_{exc} 785 nm) each positioned to probe the reaction mixture and the headspace in the cuvette above the reaction mixture. During these measurements, manual additions of solution of H_2O_2 in a prepared 1:5 (v/v) solution in CH_3CN were made by syringe injection. Analysis of headspace Raman spectra is described in the Supporting Information (Figure S3).

Raman Spectroscopy (λ_{exc} 355 nm). A stock solution containing the catalyst was prepared in CH_3CN [5 mM, 3.38

https://doi.org/10.1021/acscatal.3c00866
ACS Catal. 2023, 13, 6403−6415

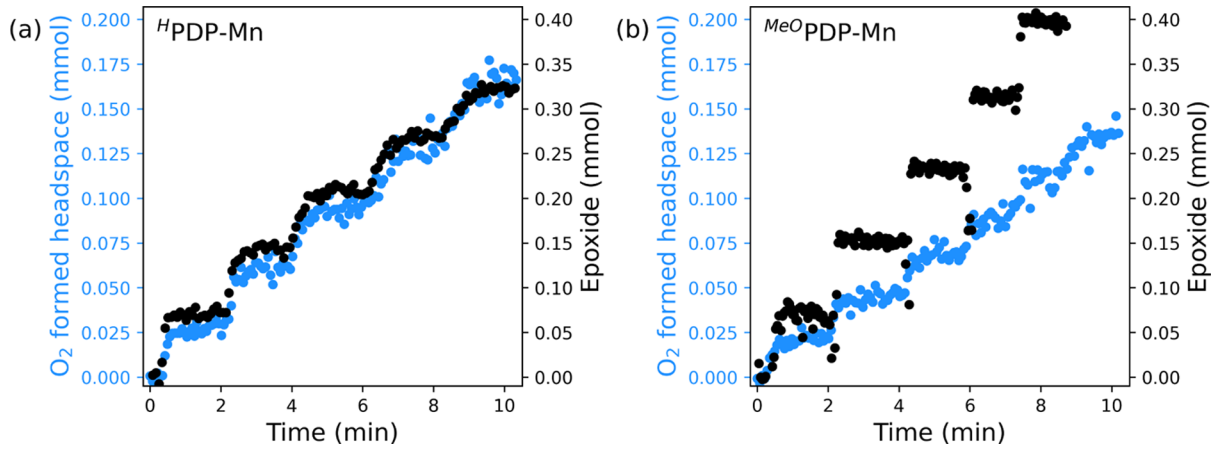

Figure 2. Formation of epoxide over time in mmol (black) and increase of O_2 in the headspace in mmol (blue) with (a) **^{H}PDP-Mn** and (b) **^{MeO}PDP-Mn** (0.5 M styrene, 1 mM catalyst, 2 M AcOH, 0.2 equiv H_2O_2 per addition), monitored by Raman spectroscopy at 785 nm (solution and headspace) at 20 °C.

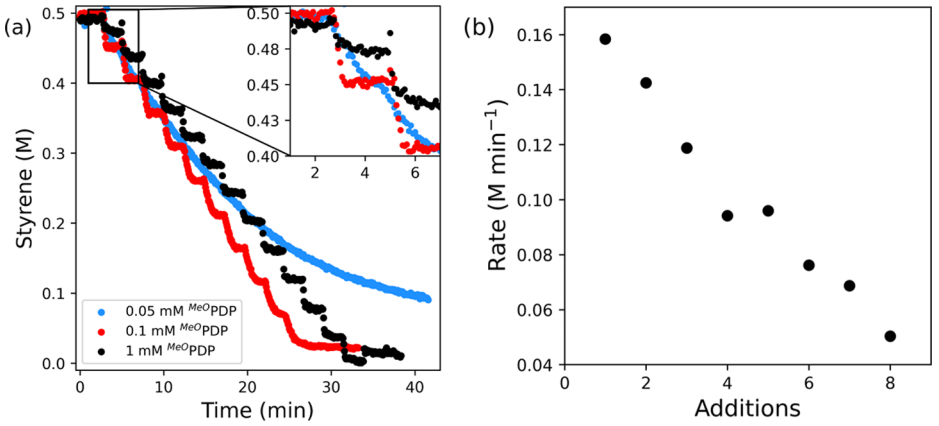

Figure 3. (a) Concentration of styrene in the epoxidation reaction catalyzed by **^{MeO}PDP-Mn** (0.05−1 mM) with 2 M AcOH, 0.135 equiv H_2O_2 drop^{-1} (average: 0.06 equiv H_2O_2 min^{-1}), monitored by Raman spectroscopy at 785 nm at 20 °C. (inset) Expansion of the initial part of the figure. Epoxide concentration over time is shown in Figure S8. (b) Observed rates of styrene conversion after each addition of H_2O_2, calculated from the conversion between three data points with 0.1 mM **^{MeO}PDP-Mn**.

mg of (**^{H}PDP-Mn**) in 1 mL of CH_3CN]. Reaction mixtures (1.5 mL total) were prepared with or without styrene (0.5 M, 86 μL), AcOH (2 M, 172 μL), and catalyst (4 mM, 1200 μL from stock solution) in CH_3CN. Raman spectra (λ_{exc} 355 nm) were recorded before and after the addition of 0.1 M H_2O_2 to this mixture [from a 50% (w/w) solution in H_2O] mixed with CH_3CN in a 1:1 (v/v) ratio.

RESULTS AND DISCUSSION

The catalysts **^{H}PDP-Mn** and **^{MeO}PDP-Mn** were chosen in this study due to the differences in enantioselectivity, as well as the TON observed earlier.[27] They are characterized by UV/vis absorption and EPR spectroscopy in solution and FTIR and Raman spectroscopy in the solid state. In acetonitrile, the catalysts show absorption in the UV region assigned to the $\pi-\pi^*$ transitions expected from the pyridine moiety (Figure S4). The complexes do not show absorption in the visible region consistent with a Mn^{II} oxidation state, and the absence of a well-defined six-line signal in the X-band EPR spectra of the complexes (Figure S5) is consistent with the deviation from octahedral (O_h) symmetry and the absence of nonligand-bound Mn^{II} ions in solution. The solid-state FTIR and Raman spectra of **^{H}PDP-Mn** and **^{MeO}PDP-Mn** are similar with expected minor differences due to the methoxy substituent (Figures S6 and S7).

Epoxidation of Styrene under Continuous Addition of H_2O_2 at Ambient Temperature. Styrene was selected as a model substrate since the Raman scattering cross-section of styrene and styrene oxide (the product) facilitates monitoring of reaction progress with H_2O_2 added dropwise over time, when catalyzed by **^{R}PDP-Mn**. The conversion of the substrate and formation of epoxide were determined by integration of the bands at 1633 and 1254 cm^{-1}, respectively (Figure S2). Furthermore, styrenes are used typically in the development of enantioselective epoxidations with this class of catalysts, and hence styrene generally provides conversions and yields representative of commonly used substrates.

The conversion of styrene to styrene oxide proceeded in a stepwise manner, i.e., a burst of activity was observed with the addition of each dose of H_2O_2 to the reaction mixture. Full conversion of styrene is reached with 1 mM catalyst in both cases (Figure 1a); however, it was reached with the **^{MeO}PDP-Mn** catalyst sooner than with the **^{H}PDP-Mn** catalyst, which reflects better efficiency in H_2O_2 usage (41 and 29%, respectively) rather than implying that the former is intrinsically a more active catalyst than the latter. Notably, the

https://doi.org/10.1021/acscatal.3c00866
ACS Catal. 2023, 13, 6403−6415

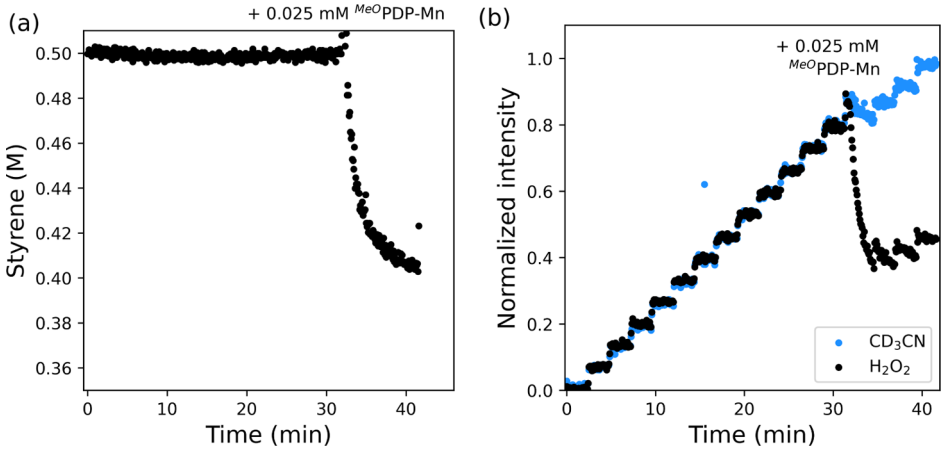

Figure 4. (a) Concentration over time of styrene with ^{MeO}**PDP-Mn** (0.01 mM) and 2 M AcOH in CH_3CN with the addition of H_2O_2 in CD_3CN (0.135 equiv H_2O_2 drop^{-1}—average: 0.06 equiv H_2O_2 min^{-1}). At 30 min, additional ^{MeO}**PDP-Mn** was added (final concn 0.035 mM), monitored by Raman spectroscopy at 785 nm at 20 °C. (b) Normalized intensity of the Raman band at 878 cm^{-1} H_2O_2 (black) and 2116 cm^{-1} CD_3CN (blue) used as diluents to determine the amount added with each drop. The loss in H_2O_2 at ca. 30 min appears incomplete due to overlap with the Raman band of acetic acid at ca. 895 cm^{-1}, which shifts toward the Raman band of H_2O_2 at 870 cm^{-1} due to the addition of water. Epoxide concentration over time is shown in Figure S8.

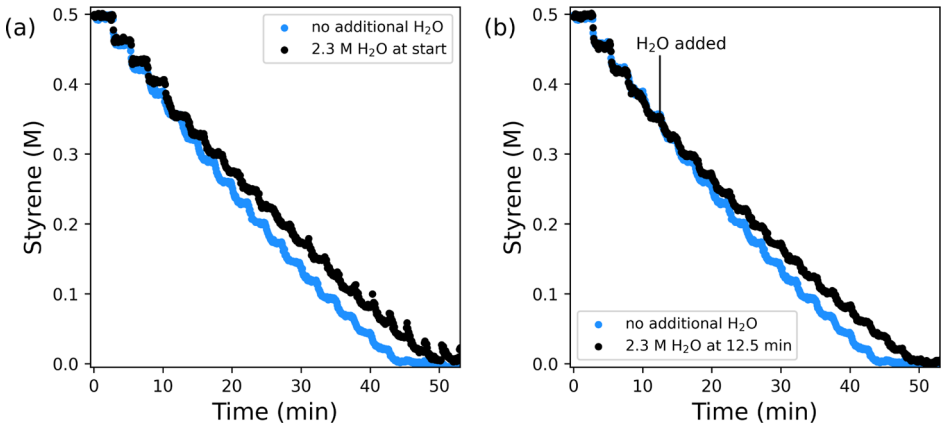

Figure 5. Concentration of styrene over time with an initial concentration of 0.5 M styrene with 1 mM ^{H}**PDP-Mn**, 2 M AcOH, 0.135 equiv H_2O_2 drop^{-1} (average 0.06 equiv H_2O_2 min^{-1}) with 2.3 M H_2O added at (a) the start and (b) at 12.5 min, monitored by Raman spectroscopy at 785 nm at 20 °C.

consumption of H_2O_2 continued after full conversion of the substrate. With a reduced catalyst concentration (0.1 mM, Figure 1b), the TON achieved with ^{H}**PDP-Mn** was 2600, while for ^{MeO}**PDP-Mn**, the TON was limited to 5000 (full conversion of alkene) with 81% efficiency with respect to H_2O_2.

The observed rate of the reaction was estimated from the changes in Raman scattering intensity that follow the individual additions of H_2O_2. It is apparent that the ^{MeO}**PDP-Mn** catalyst consumes the H_2O_2 added with each drop within 10 s (TOF > 5 s^{-1}), whereas the ^{H}**PDP-Mn** catalyst requires 30 s (TOF > 1 s^{-1}) to consume the same amount of H_2O_2 (Figure 1). The release of O_2 was found, by headspace Raman spectroscopy, to proceed in a stepwise manner concomitant with the formation of styrene epoxide and occurs already at the first addition of H_2O_2 (Figure 2). The simultaneous formation of O_2 with alkene oxidation is notable, and the constant relative efficiency over the duration of the reaction indicates that disproportionation of H_2O_2 is not due to manganese species released by decomposition of the catalyst but due to competition between styrene and H_2O_2 as substrates for the activated catalyst. For ^{H}**PDP-Mn**, a similar amount of H_2O_2 is used to oxidize styrene as is disproportionated to O_2 (0.32 mmol epoxide, 0.16 mmol O_2 from 2 equiv H_2O_2), whereas for ^{MeO}**PDP-Mn**, almost twice as much H_2O_2 is used for styrene oxidation than disproportionation (0.40 mmol epoxide, 0.13 mmol O_2 from 2 equiv H_2O_2, Figure S8).

The conversion of styrene to styrene oxide shows a complex dependence on the concentration of ^{MeO}**PDP-Mn** (Figure 3a). The maximum rate of conversion and efficiency is obtained with 0.1 mM catalyst. When the concentration of the catalyst is 0.05 mM, the observed rate of oxidation of alkene with each addition of H_2O_2 is lower than when it is 0.1 mM. However, the efficiency in regard to the oxidant is the same at both catalyst concentrations. The reaction rate observed after each H_2O_2 addition with the 0.05 mM catalyst, however, decreases more rapidly, and eventually catalyst deactivation leads to a build-up of H_2O_2. Surprisingly, with 1 mM catalyst, the efficiency with respect to H_2O_2 and observed rate of conversion of alkene is lower than that with 0.1 mM catalyst due to a change in the relative rate of disproportionation and

https://doi.org/10.1021/acscatal.3c00866
ACS Catal. 2023, 13, 6403−6415

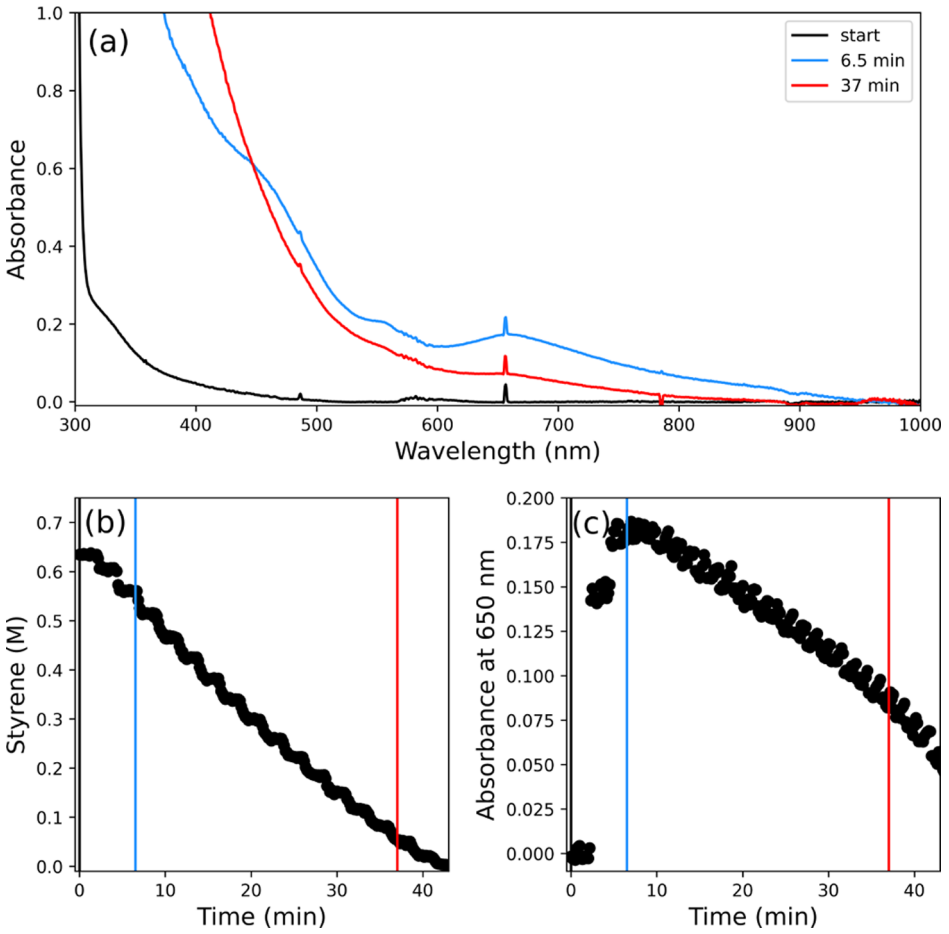

Figure 6. (a) UV/vis absorption spectra recorded under reaction conditions [0.5 M styrene, 1 mM ^{H}**PDP-Mn**, 2 M AcOH, 0.135 equiv H_2O_2 drop^{-1} (average: 0.06 equiv H_2O_2 min^{-1}) at 20 °C] at t = 0 (black), t = 6.5 min (blue), and t = 37 min (red), (b) corresponding plot of styrene concentration over time determined by Raman spectroscopy λ_{exc} 785 nm, and (c) absorbance at 650 nm over time. The sharp feature at 656 nm is an artifact due to a D_2 emission line.

alkene oxidation rather than reduced overall catalytic activity. With 1 mM ^{MeO}**PDP-Mn**, the consumption of H_2O_2 is complete within the time resolution of the Raman spectrometer (ca. 8 s). The efficiency with respect to styrene oxidation overall, however, indicates that H_2O_2 disproportionation becomes relatively more important at higher concentrations of the catalyst. With 0.1 mM catalyst, the observed rate estimated for each addition (drop) of H_2O_2 decreases as the reaction proceeds by a factor of four over eight additions, indicating a steady loss in catalyst activity (Figure 3b).

With the 0.01 mM catalyst, little to no conversion is observed under continuous dropwise addition of the oxidant (Figures 4 and S8). Subsequent addition of the catalyst (to a total concn of 0.035 mM) to the reaction mixture resulted in substantial conversion (25%) of styrene to its epoxide, much more than that which can be accounted for by the H_2O_2 added after 30 min. Hence, the rapid conversion confirms that the 1.5 equiv H_2O_2 added steadily over the first 30 min was not consumed significantly by disproportionation. Hence, it can be concluded that immediate deactivation of the catalyst toward styrene oxidation also inactivates it toward disproportionation of H_2O_2. Overall, the data indicates that the catalyst is responsible for both oxidation of the substrate and disproportionation of H_2O_2, but it is not possible to conclude nor exclude that the same reactive species that engages with the alkene substrate also engages with H_2O_2. It is clear although that catalyst deactivation affects both reaction pathways.

The concentration of water increases over the duration of the reaction as it is added both with H_2O_2 and is produced as H_2O_2 is consumed in epoxidation and disproportionation. Indeed, the concentration of H_2O eventually exceeds that of the acetic acid present, prompting consideration of the effect of water concentration on catalytic activity. Reactions, in which the concentration of water already at the start was ca. 2.3 M (Figure 5a), as well as addition of water to 2.3 M after 5 min (Figure 5b), show that the efficiency in the use of H_2O_2 was reduced. The overall increase in reaction "time" needed to achieve full conversion is therefore due to the decrease in selectivity for alkene epoxidation over disproportionation of H_2O_2, resulting in the need to add H_2O_2 for a longer period.

In summary, reaction progress monitoring reveals that ^{H}**PDP-Mn** and ^{MeO}**PDP-Mn** both disproportionate H_2O_2 and epoxidize styrene, reaching a TOF toward epoxidation of 3 s^{-1} with ^{H}**PDP-Mn** and 10 s^{-1} with ^{MeO}**PDP-Mn** (Figure S9). It appears that the active form of the catalyst ^{MeO}**PDP-Mn** reacts faster with the substrate than with H_2O_2 realizing greater efficiency in epoxidation. The release of O_2 concomitant with the conversion of the alkene to the epoxide indicates that alkene and H_2O_2 compete as substrates for the same reactive species.[35,36] Furthermore, it is apparent that the macroscopic rate observed is determined by mass transport (rate of mixing)

https://doi.org/10.1021/acscatal.3c00866
ACS Catal. 2023, 13, 6403−6415

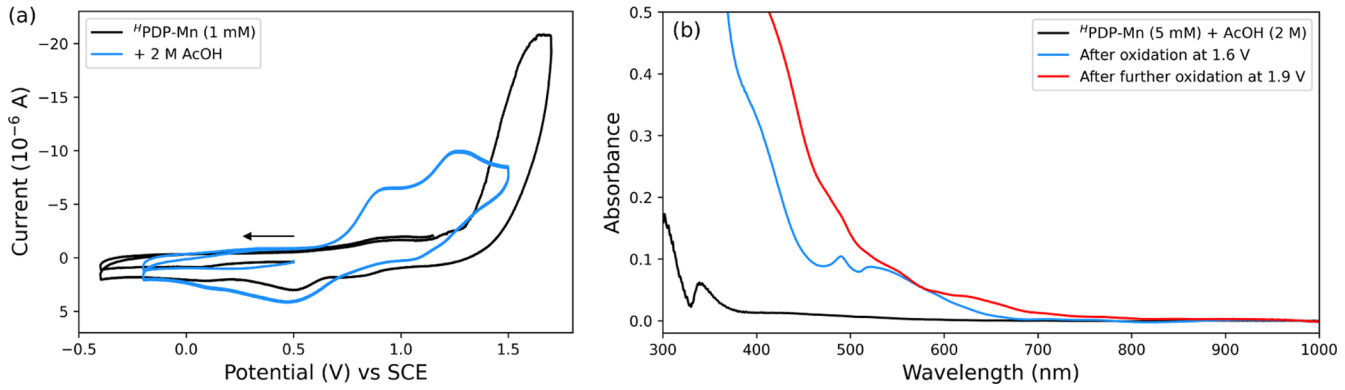

Figure 7. (a) Cyclic voltammetry (0.1 V s^{-1}) of **^{H}PDP-Mn** (1 mM) in CH_3CN (0.1 M KPF_6) (black) and with (blue) 2 M AcOH. (b) UV/vis absorption spectrum of (black) HPDP-Mn (5 mM) with acetic acid (2 M) in CH_3CN, (blue) after oxidation at 1.6 V and (red) further oxidation at 1.9 V. See the Supporting Information for further details.

and underestimates the maximum rate of the reaction that can be achieved. Ultimately, the deactivation of the catalyst, as well as disproportionation of H_2O_2, limits the extent of epoxidation of styrene and hence differences in overall alkene conversion introduced by substituents on the ligand of the catalyst need to be interpreted with caution in regard to intrinsic reactivity of the catalyst. Furthermore, the question arises as to the nature of the "deactivated" species, whether it involves the formation of complexes that are resting states or if ligand decomposition occurs.[37,38]

UV/Vis Absorption, EPR, and Resonance Raman Spectroscopy under Reaction Conditions. Although the (pre)catalysts used are mononuclear Mn^{II} complexes, their oxidation state and nuclearity during the reaction are not yet established nor has the detailed role(s) of the carboxylic acid, that is essential to the reactivity, been fully elucidated. Indeed, through the addition of H_2O_2, at least transient formation of higher oxidation states would be expected, which generally show significant visible absorption.[39−41] Hence, in situ spectroscopy during oxidation was applied to explore the species formed under various reaction conditions with direct correlation with substrate conversion.

Under the reaction conditions discussed above (at room temperature), dropwise addition of H_2O_2 results in changes to the UV/vis absorption spectrum of the reaction mixture (Figure 6). Initially, the visible absorption spectrum is featureless, consistent with the Mn^{II} oxidation state of the catalysts (Figure S4). Absorption bands in the UV region are assigned to the substrate (styrene) and the $\pi-\pi^*$ transition of the PDP ligands.

Over the first 6.5 min following two additions of H_2O_2 to **^{H}PDP-Mn**, an increase in absorption in the near UV and the appearance of weaker visible absorption bands occur. The visible absorption spectrum shows a maximum absorbance at 660 nm (molar absorptivity of 185−370 M^{-1} cm^{-1}, assuming full conversion of the catalyst to a monomeric or dimeric species) with shoulders at 556 and 454 nm and is the same as that observed under reaction conditions with **^{MeO}PDP-Mn** (Figures S10 and S11). The UV/vis absorption spectrum and molar absorptivities are consistent with Mn^{III}/Mn^{IV} species.[42−45] X-band EPR spectra recorded for samples frozen after the addition of three drops of H_2O_2 and close to the point of maximum absorbance at 660 nm show the characteristic 16-line signal (ca. 75 G peak to peak separation) of a $Mn_2^{III,IV}$ μ-oxido bridged dimer (Figure S12) and the signal intensity is consistent with the catalyst concentration (maximum 0.5 mM dimer).[38,42,43,46] The visible absorption bands decrease over the course of the reaction, indicating conversion to other species (Figure 6a), likely still in a Mn^{III} or Mn^{IV} oxidation state given the persistence of an intense near UV absorption, indicating a shift in the equilibrium between several species present under reaction conditions. Such mononuclear Mn^{III} and dinuclear $Mn_2^{III,III}$ species will be EPR silent (perpendicular mode). The species observed are reminiscent to those reported recently by Rybak-Akimova and coworkers[41] for related pyridyl-amine catalysts during epoxidation of alkenes with H_2O_2.

The same visible absorption spectrum appears already after the addition of a few equivalents of H_2O_2, indicating that the formation of these dinuclear complexes from Mn^{II} occurs within a few turnovers of the catalyst (Figure S13). Interestingly, at a lower concentration of acetic acid (0.1 M), the formation of the same $Mn_2^{III,IV}$ complex is significantly slower (from 30 s to more than 10 min, Figure S13, inset). It is notable that these species are generated after multiple turnovers of the catalyst, and although they represent the main part of the manganese complexes present, they are not necessarily directly involved in the catalytic cycle. Indeed, the lack of correlation between appearance and catalytic activity points to the complexes being inactive in catalysis.

A key feature of the chemistry of the **^{R}PDP-Mn** catalysts is the need for excess acetic acid to see alkene epoxidation. In the absence of acetic acid, the absorption spectrum of the reaction mixture does not change significantly upon addition of H_2O_2. Addition of acetic acid after addition of H_2O_2 results in immediate appearance of the same absorption spectrum observed when acid was present prior to adding H_2O_2 (Figure S14). Additional H_2O_2 was not needed to induce this change, confirming that decomposition of H_2O_2 was not significant prior to adding acetic acid either. Hence, it can be surmised that one of the roles played by acetic acid in the catalysis is to facilitate initial oxidation of the catalysts with H_2O_2. Cyclic voltammetry (vide infra) is in agreement with this conclusion.

Cyclic Voltammetry and (Spectro)electrochemistry. In CH_3CN, **^{H}PDP-Mn** shows a chemically irreversible oxidation at 1.6 V vs SCE assigned to a Mn^{II}/Mn^{III} redox couple, which is followed by a series of reductions at 0.8, 0.5, and 0.1 V on the return cycle toward negative potentials (Figures 7 and S15−S18). Addition of acetic acid (2.0 M) changes the voltammetry with quasi-reversible redox waves at

https://doi.org/10.1021/acscatal.3c00866
ACS Catal. 2023, 13, 6403−6415

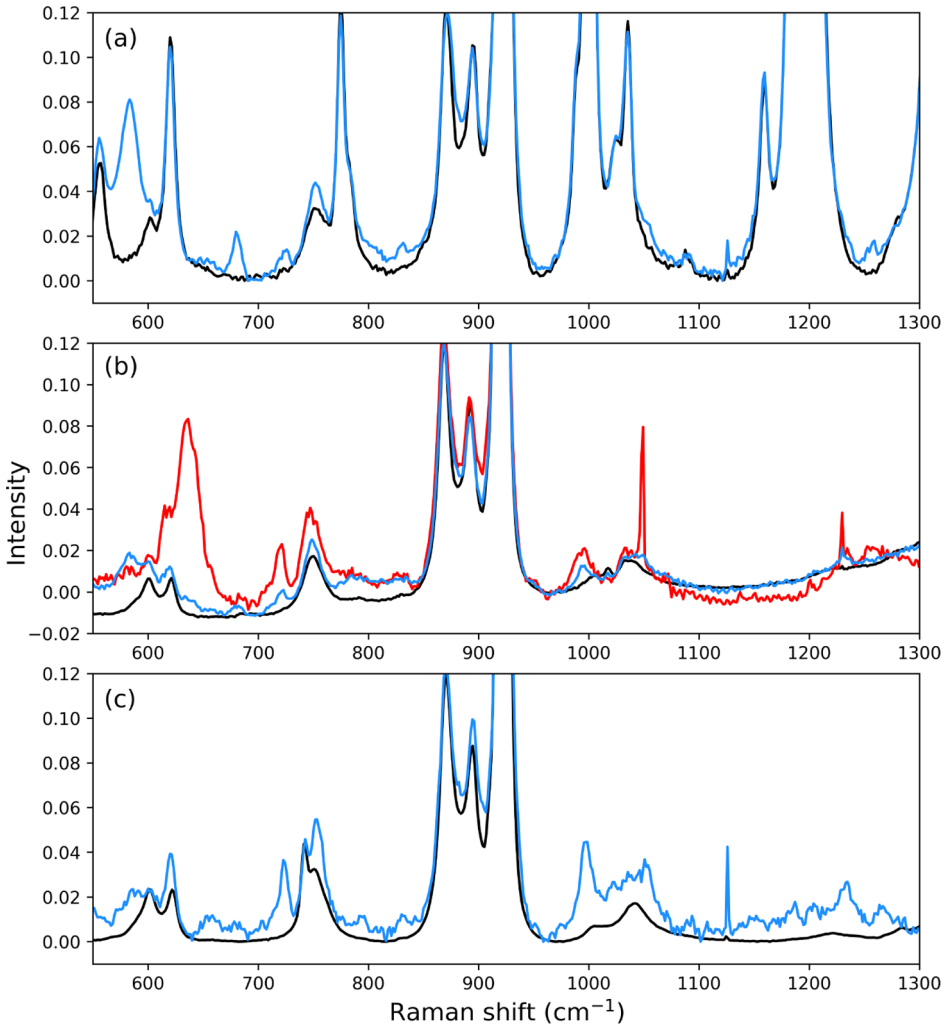

Figure 8. Raman spectra (λ_{exc} 355 nm) recorded at 20 °C (a) under reaction conditions (0.5 M styrene, 4 mM **^{H}PDP-Mn**, 2 M AcOH) before (black) and after (blue) the addition of H_2O_2 (to 0.1 M), (b) in the absence of the substrate (4 mM **^{H}PDP-Mn**, 2 M AcOH, 0.1 M H_2O_2) before (black), directly after the addition of H_2O_2 (to 0.12 M, red) and after 3 min (blue), and (c) after electrochemical formation of a $Mn_2^{III,III}$ species from 4 mM **^{H}PDP-Mn**, 2 M AcOH in CH_3CN (0.1 M KPF_6). The spectra in (a) are shown in Figure S22 with the spectrum of solvent to facilitate viewing of the additional band.

0.7 and at 1.2 V, consistent with the exchange of solvent (e.g., CH_3CN) ligands for acetate observed by electrospray ionization-mass spectrometry (vide infra), but the open-circuit potential and colorless solution indicate that the complex remains in the Mn^{II} oxidation state. Addition of H_2O_2, after acetic acid, results in a colored solution (Figure S19, vide infra) and a positive shift in open-circuit potential (Figure S17), both consistent with a change in oxidation state, i.e., to Mn^{III} and/or Mn^{IV} species, but importantly, voltammetry is otherwise unaffected (see the Supporting Information for detailed discussion).

Bulk electrochemical oxidation of **^{H}PDP-Mn** in CH_3CN in the presence of acetic acid (Figure 7) results in the appearance of visible absorption bands with maxima at 490 and 525 nm typical of a μ-oxido bridged dinuclear Mn^{III} complex in terms of the shape of the visible absorption bands and the molar absorptivity (210 M^{-1} cm^{-1} at 490 nm).[47−49] Oxidation at more positive potential results in a further increase in near-UV and -visible absorbance resulting ultimately in a spectrum that resembles the spectra obtained under reaction conditions with styrene present (vide supra, Figure 6). Subsequent reduction at ca. 0.0 V results in a substantial decrease in near-UV and -visible absorption. The spectrum is recovered quantitatively upon reoxidation; however, bands of the Mn_2^{III} species formed initially did not reappear during the stepwise oxidation on the second cycle (Figure S20).

In the absence of the substrate (styrene), the UV/vis absorption spectrum also changes upon addition of H_2O_2; however, the most significant spectral features are at 490 nm with two shoulders at 410 and 540 nm, which are similar to the spectrum generated initially during spectroelectrochemistry (i.e., a dinuclear Mn^{III} species, vide supra, Figure S21). Subsequent addition of styrene had relatively little effect on the spectrum; however, a further addition of H_2O_2 results in a change to a spectrum that more closely resembles that obtained with styrene present initially (increased absorbance at 700 nm). Overall, the spectral changes observed indicate that there is a driving force for formation of dinuclear complexes[41] upon oxidation to Mn^{III} and Mn^{IV} oxidation states either electrochemically or with H_2O_2 in the presence of acetic acid and that multiple structures are present in equilibrium in solution.

Resonance enhancement of Raman bands of the catalyst at 355 nm confirms the presence of several species depending on

https://doi.org/10.1021/acscatal.3c00866
ACS Catal. 2023, 13, 6403−6415

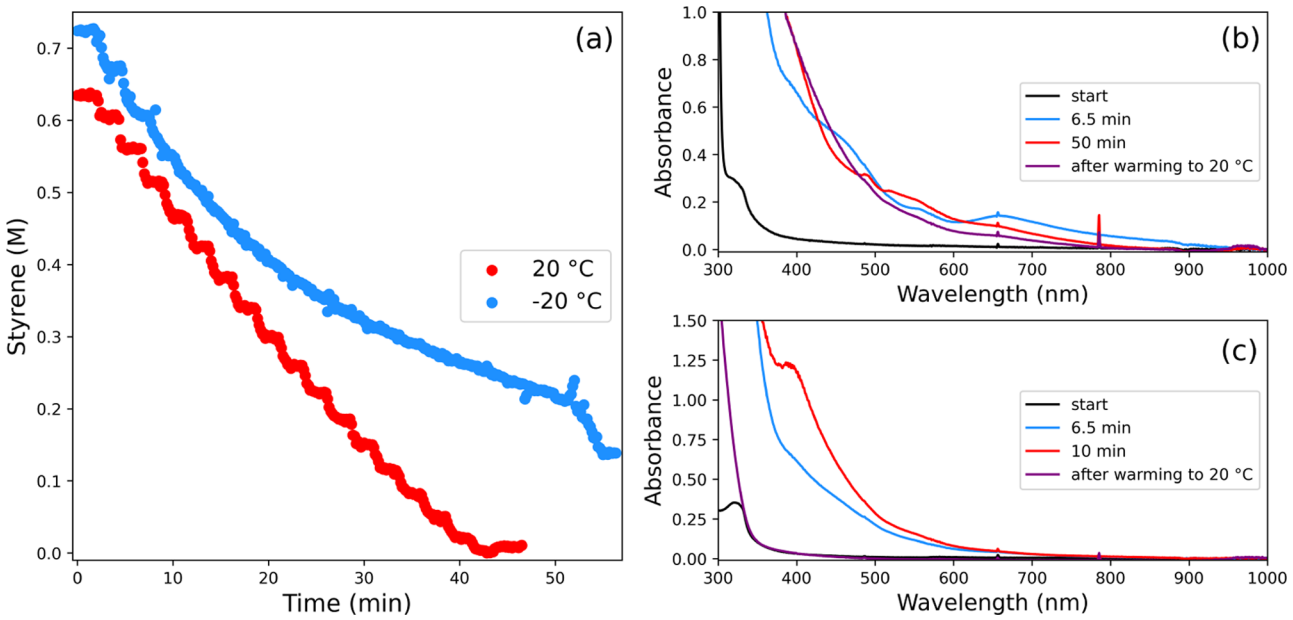

Figure 9. (a) Oxidation of styrene over time with 0.5 M styrene, 1 mM ^{H}**PDP-Mn**, 2 M AcOH, 0.135 equiv H_2O_2 drop^{-1} (average: 0.06 equiv H_2O_2 min^{-1}), monitored using Raman spectroscopy at 785 nm at 20 °C (red) and −20 °C (blue), corresponding epoxide concentration in Figure S24. (b) Absorption spectra in the same experiment at −20 °C at t = 0 (black), t = 6.5 min (blue), and t = 50 min (red) and after warming to r.t. (purple). (c) Absorption spectra at −20 °C in the absence of the substrate (1 mM ^{H}**PDP-Mn**, 2 M AcOH), 0.135 equiv H_2O_2 drop^{-1} (average: 0.06 equiv H_2O_2 min^{-1}) at t = 0 (black), t = 6.5 min (blue), and t = 10 min (red) and after warming to r.t. (purple).

Scheme 3. Initial Oxidation of Mn^{II} Catalysts by H_2O_2 in the Presence of Acetic Acid and Interconnected Reaction Pathways[a]

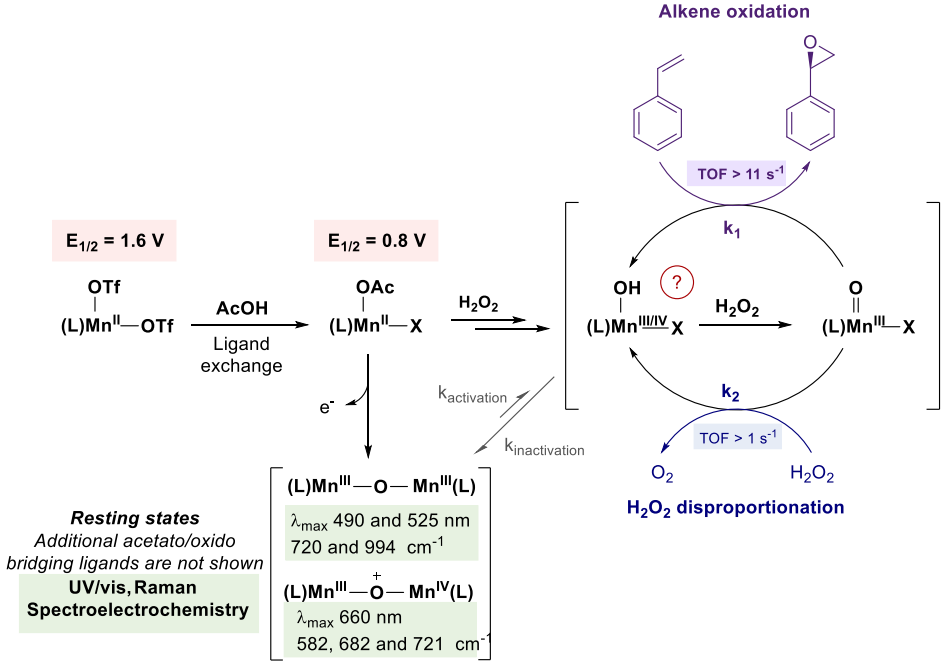

[a]Species observed in the reaction mixture during catalysis spectroscopically can be generated electrochemically also. Note that assignment of the structures of resting states to specific oxido/acetato bridged structures can be made tentatively by comparison with known complexes of related ligands; however, under reaction conditions, a mixture of structures are certainly present, dependent on the conditions and presence of substrate, with additional acetate and oxido bridging or monodentate ligands (not shown).

the conditions used. The characteristic band of styrene epoxide at 1254 cm^{-1} appears within 25 s of addition of H_2O_2 (Figure 8a); however, in contrast to nonresonant Raman spectra of the reaction mixture obtained with 785 nm excitation, with 355 nm excitation, additional bands appear at 582, 682, and 721 cm^{-1}. In the absence of styrene (Figure 8b), immediately after the addition of H_2O_2, bands appear at 636, 720, and 994 cm^{-1}. Within 2 min, the band at 636 cm^{-1} had disappeared with the bands at 720 and 994 cm^{-1} persisting. This latter species is observed in the Raman spectrum obtained by electrochemical oxidation (Figure 8c). It is notable that the spectra are different to those obtained with styrene present.

https://doi.org/10.1021/acscatal.3c00866
ACS Catal. 2023, 13, 6403−6415

These data indicate that although recognizable dinuclear complexes form under reaction conditions, a dynamic equilibrium between multiple species is established rather than any one complex forming a thermodynamic trap. Their generation electrochemically as well as with H_2O_2 establishes that ligand degradation is not involved in their formation as does high-resolution mass spectrometry data that correspond to a $[Mn^{II}(^{H}PDP)(OAc)]^+$ species present before and after catalysis (Figure S23).

Reactivity at Low Temperature. Earlier reports have shown that at subambient temperatures, both conversion of styrene and enantioselectivity are improved.[15] Comparison of the conversion of styrene over time at 20 °C and at −20 °C shows that the initial observed rate of the reaction is the same at both temperatures. The UV/vis absorption spectrum obtained during the reaction at −20 °C shows the same features of the $Mn^{III,IV}$ species observed at 20 °C. However, at −20 °C, the observed reaction rate toward epoxidation following each dose of H_2O_2 decreases much more rapidly than that at 20 °C (Figures 9 and S24). Furthermore, the UV/vis absorption spectrum of the reaction mixture changes to resemble more the Mn^{III} species that were observed at 20 °C without the substrate present (vide supra). It is also notable that the extent of conversion reached at −20 °C is lower than at 20 °C; however, upon warming of the reaction mixture from −20 to 20 °C, a sudden increase in conversion of styrene was observed as was conversion of H_2O_2, indicating that the loss of activity was not due to increased competition from disproportionation of H_2O_2. The change in UV/vis absorption spectrum from one that is characteristic of a $Mn_2^{III,IV}$ species to that of a $Mn_2^{III,III}$ species and subsequently on warming to a $Mn_2^{III,IV}$ species provides strong evidence that $Mn_2^{III,III}$ is an inactive/resting state of the catalyst. The benefit of reduced temperature is therefore more likely due to a reduction in H_2O_2 disproportionation relative to alkene oxidation, e.g., in an opposite manner to the effect of addition of water (vide supra). From a broader perspective, the sudden increase in activity upon warming may impact efforts to follow the reaction progress at low temperature by off-line analysis methods.

Summary and Mechanistic Considerations. The findings discussed above are summarized in Scheme 3. With dropwise addition of H_2O_2, which is used typically for the class of catalysts studied here, the time taken for full conversion of the substrate is determined by the rate of addition of the oxidant and eventually the rate of catalyst deactivation. In situ Raman spectroscopy reveals the actual activity of the catalysts. We show that each drop of the oxidant containing solution results in a short burst of substrate oxidation/H_2O_2 disproportionation, with TOFs (>10 s^{-1}) that are much greater than that would be expected from the overall reaction time. The differences in the TOF determined for two examples of this class of the catalyst indicate that overall conversion is dictated by efficiency in H_2O_2 (i.e., limited by competing H_2O_2 disproportionation after each addition) and by catalyst deactivation rather than intrinsic reactivity. **^{MeO}PDP-Mn** is more efficient than **^{H}PDP-Mn** in the use of H_2O_2 for epoxidation and shows a lower rate of catalyst deactivation. Hence, the effect of substituents overall is the net result of their impact on each of these processes.

Drawing conclusions as to the effect of substituents assumes that the active species is not formed upon degradation of the ligand as observed elsewhere for pyridyl amine-based ligands.[37,38,50] In this regard, enantioselectivity is key evidence of the structural integrity of the PDP ligands during the catalysis. However, the species responsible for disproportionation of H_2O_2 are less readily identified. In situ reaction monitoring reveals that the catalyst rather than catalyst decomposition products are responsible for H_2O_2 disproportionation, i.e., both styrene and H_2O_2 are substrates for the catalyst. The difference in efficiency in the initial stages of the reaction provides good insight into the effect of substituents in controlling selectivity between H_2O_2 disproportionation and alkene epoxidation. It should be noted that it cannot be ascertained whether the same reactive species is responsible for both reactions or whether two distinct reactive species are in equilibrium in the reaction mixture.

Introducing the methoxy substituent on the ligand results in increased reactivity; the rate of consumption of H_2O_2 for both disproportionation and epoxidation but still favoring the latter reaction. This observation substantiates previous interpretations solely based on epoxide yields at the end of reactions.[27] We note that the observation is in apparent contradiction with results of the Hammett analysis, by Bryliakov and coworkers,[28] of the oxidation of *para*-substituted chalcones with the catalyst **^{H}PDP-Mn**, which indicated that the oxygen atom-transferring species is electrophilic. The electron-donating *p*-methoxy substituent on the ligand would reduce electrophilicity. Along this line, improvements in enantioselectivity in epoxidation reactions upon introducing electron-releasing groups in the pyridine rings of the catalysts have also been previously interpreted in terms of a less-electrophilic manganese-oxo species that undergoes oxygen atom transfer via a later transition state.[27,29] However, the rate-controlling step in the reaction is likely not the oxygen atom transfer step but rather either binding of H_2O_2 to the manganese complex, or O−O bond cleavage, which may be facilitated by a more electron-rich manganese center.

Raman and UV/vis spectroscopy confirms that multiple species are present throughout the reaction in various ratios (Scheme 3). Indeed, spectroscopic analysis of the reaction mixture over time together with (spectro)electrochemical data indicates that acetic acid enables oxidation of the Mn^{II} catalysts to their Mn^{III} and Mn^{IV} oxidation states and the onset of catalytic activity; however, the observation of such species does not necessarily imply their involvement in the catalytic cycle (Scheme 3). The Mn^{III} species observed are stable resting states and that during catalysis, there are several distinct complexes present in equilibrium. Hence, there are two pathways that lead to deactivation under reaction conditions. The first is the reversible formation of inactive species (e.g., dinuclear $Mn^{III/IV}$ complexes) in which the ligand is unaffected and the catalyst can recover to an active form. Indeed, it is worth noting that covalent immobilization of related manganese catalysts by Sun and coworkers[51,52] in a porous organic polymer support allows for recovery and reuse of the catalysts over multiple cycles. The dispersion of the catalyst in such a case likely inhibits formation of multinuclear complexes. The second deactivation pathway is irreversible and likely involves ligand loss and decomposition. However, at lower temperatures, this pathway is less apparent and hence understanding how, for example, steric interactions can prevent formation of inactive complexes in the first place may help in understanding differences substituent variations make in determining catalyst performance.

https://doi.org/10.1021/acscatal.3c00866
ACS Catal. 2023, 13, 6403−6415

CONCLUSIONS

The ^{R}PDP-Mn family of complexes provides for high yields and TONs and excellent enantioselectivities in the epoxidation of alkenes. Enantioselectivities and yields are tuned by variation in ligand substituents to tune the electronic properties of the reactive manganese centers. We show in the present work that efficiency in the oxidant (H_2O_2) is dependent on competition of the alkene and H_2O_2 as substrates for the reactive species and the selectivity between these two substrates is dependent on electronic factors. Hence, although correlations between TON and ligand substituent can be drawn from the overall outcome of the reactions, it is important to recognize that the main determinants in alkene conversion are the selectivity between alkene and H_2O_2 as substrates and also the rate of deactivation of the catalyst. A priori it cannot be assumed that substituents affect both aspects in a similar manner.

As a final point, a common approach of H_2O_2 is to use subambient temperatures, thereby reducing the rate of catalyst decomposition to species that can engage in H_2O_2 disproportionation. The observations made here that the same species is responsible for disproportionation as is for alkene oxidation and that the deactivated catalyst is not responsible for either reaction do not mean that the approach is without merit. For the ^{R}PDP-Mn complexes, lowering temperature shifts the H_2O_2/alkene selectivity in favor of the latter. However, the rate of deactivation is increased and a build-up of H_2O_2 can occur, which on warming and reactivation of the catalyst lead to a burst of reactivity at higher temperature, potentially negating the benefit of lower temperatures on enantioselectivity. Such behavior may be of relevance in other systems.

ASSOCIATED CONTENT

Supporting Information

The Supporting Information is available free of charge at https://pubs.acs.org/doi/10.1021/acscatal.3c00866.

Additional electrochemical, spectroscopic, and reaction monitoring data (PDF)

AUTHOR INFORMATION

Corresponding Authors

Miquel Costas − *Institut de Química Computacional i Catàlisi (IQCC) and Departament de Química, Universitat de Girona, Girona E-17071 Catalonia, Spain;* orcid.org/0000-0001-6326-8299; Email: Miquel.costas@udg.edu

Wesley R. Browne − *Molecular Inorganic Chemistry, Stratingh Institute for Chemistry, Faculty of Science and Engineering, University of Groningen, 9747AG Groningen, The Netherlands;* orcid.org/0000-0001-5063-6961; Email: w.r.browne@rug.nl

Authors

Johann B. Kasper − *Molecular Inorganic Chemistry, Stratingh Institute for Chemistry, Faculty of Science and Engineering, University of Groningen, 9747AG Groningen, The Netherlands*

Laia Vicens − *Institut de Química Computacional i Catàlisi (IQCC) and Departament de Química, Universitat de Girona, Girona E-17071 Catalonia, Spain*

C. Maurits de Roo − *Molecular Inorganic Chemistry, Stratingh Institute for Chemistry, Faculty of Science and Engineering, University of Groningen, 9747AG Groningen, The Netherlands*

Ronald Hage − *Molecular Inorganic Chemistry, Stratingh Institute for Chemistry, Faculty of Science and Engineering, University of Groningen, 9747AG Groningen, The Netherlands; Catexel B.V., BioPartner Center Leiden, 2333BD Leiden, The Netherlands*

Complete contact information is available at: https://pubs.acs.org/10.1021/acscatal.3c00866

Author Contributions

The manuscript was written through contributions of all authors. All authors have given approval to the final version of the manuscript.

Notes

The authors declare no competing financial interest.

ACKNOWLEDGMENTS

Financial support was provided by the Ministry of Education, Culture and Science of the Netherlands (Gravity Program 024.001.035 to W.R.B.) and the Advanced Research Center Chemical Building Blocks Consortium (2021.038.C.RUG.8). Support by the Spanish Ministry of Science, Innovation and Universities; (PhD grant FPU16/04231 to L.V.) and Generalitat de Catalunya (ICREA Academia Award to M.C. and 2017 SGR 00475) is acknowledged.

REFERENCES

(1) Bäckvall, J. *Modern Oxidation Methods*; Bäckvall, J.-E., Ed.; Wiley-VCH Verlag GmbH & Co. KGaA: Weinheim, FRG, 2004; pp 1−465.

(2) Dalton, T.; Faber, T.; Glorius, F. C.-H. C−H Activation: Toward Sustainability and Applications. *ACS Cent. Sci.* **2021**, *7*, 245−261.

(3) Philip, R. M.; Radhika, S.; Abdulla, C. M. A.; Anilkumar, G. Recent Trends and Prospects in Homogeneous Manganese-Catalysed Epoxidation. *Adv. Synth. Catal.* **2021**, *363*, 1272−1289.

(4) Bryliakov, K. P. Catalytic Asymmetric Oxygenations with the Environmentally Benign Oxidants H_2O_2 and O_2. *Chem. Rev.* **2017**, *117*, 11406−11459.

(5) Carney, J. R.; Dillon, B. R.; Thomas, S. P. Recent Advances of Manganese Catalysis for Organic Synthesis. *Eur. J. Org. Chem.* **2016**, *2016*, 3912−3929.

(6) Son, J. Sustainable Manganese Catalysis for Late-Stage C-H Functionalization of Bioactive Structural Motifs. *Beilstein J. Org. Chem.* **2021**, *17*, 1733−1751.

(7) Irie, R.; Noda, K.; Ito, Y.; Matsumoto, N.; Katsuki, T. Catalytic Asymmetric Epoxidation of Unfunctionalized Olefins. *Tetrahedron Lett.* **1990**, *31*, 7345−7348.

(8) Irie, R.; Noda, K.; Ito, Y.; Katsuki, T. Enantioselective Epoxidation of Unfunctionalized Olefins Using Chiral (Salen)-Manganese(III) Complexes. *Tetrahedron Lett.* **1991**, *32*, 1055−1058.

(9) Zhang, W.; Loebach, J. L.; Wilson, S. R.; Jacobsen, E. N. Enantioselective Epoxidation of Unfunctionalized Olefins Catalyzed by Salen Manganese Complexes. *J. Am. Chem. Soc.* **1990**, *112*, 2801−2803.

(10) Jacobsen, E. N.; Zhang, W.; Muci, A. R.; Ecker, J. R.; Deng, L. Highly Enantioselective Epoxidation Catalysts Derived from 1,2-Diaminocyclohexane. *J. Am. Chem. Soc.* **1991**, *113*, 7063−7064.

(11) Sun, W.; Sun, Q. Bioinspired Manganese and Iron Complexes for Enantioselective Oxidation Reactions: Ligand Design, Catalytic Activity, and Beyond. *Acc. Chem. Res.* **2019**, *52*, 2370−2381.

(12) Vicens, L.; Olivo, G.; Costas, M. Rational Design of Bioinspired Catalysts for Selective Oxidations. *ACS Catal.* **2020**, *10*, 8611−8631.

(13) Murphy, A.; Dubois, G.; Stack, T. D. P. Efficient Epoxidation of Electron-Deficient Olefins with a Cationic Manganese Complex. *J. Am. Chem. Soc.* **2003**, *125*, 5250−5251.
(14) Murphy, A.; Pace, A.; Stack, T. D. P. Ligand and pH Influence on Manganese-Mediated Peracetic Acid Epoxidation of Terminal Olefins. *Org. Lett.* **2004**, *6*, 3119−3122.
(15) Ottenbacher, R. V.; Bryliakov, K. P.; Talsi, E. P. Nonheme Manganese-Catalyzed Asymmetric Oxidation. A Lewis Acid Activation versus Oxygen Rebound Mechanism: Evidence for the "Third Oxidant. *Inorg. Chem.* **2010**, *49*, 8620−8628.
(16) Ottenbacher, R. V.; Bryliakov, K. P.; Talsi, E. P. Non-Heme Manganese Complexes Catalyzed Asymmetric Epoxidation of Olefins by Peracetic Acid and Hydrogen Peroxide. *Adv. Synth. Catal.* **2011**, *353*, 885−889.
(17) Ottenbacher, R. V.; Samsonenko, D. G.; Talsi, E. P.; Bryliakov, K. P. Highly Efficient, Regioselective, and Stereospecific Oxidation of Aliphatic C-H Groups with H_2O_2, Catalyzed by Aminopyridine Manganese Complexes. *Org. Lett.* **2012**, *14*, 4310−4313.
(18) Wang, B.; Miao, C. X.; Wang, S. F.; Kühn, F. E.; Xia, C. G.; Sun, W. Non-heme manganese complexes of C1-symmetric N4 ligands: Synthesis, characterization and asymmetric epoxidations of *α,β*-enones. *J. Organomet. Chem.* **2012**, *715*, 9−12.
(19) Shen, D.; Miao, C.; Wang, S.; Xia, C.; Sun, W. Efficient Benzylic and Aliphatic C-H Oxidation with Selectivity for Methylenic Sites Catalyzed by a Bioinspired Manganese Complex. *Org. Lett.* **2014**, *16*, 1108−1111.
(20) Gómez, L.; Garcia-Bosch, I.; Company, A.; Sala, X.; Fontrodona, X.; Ribas, X.; Costas, M. Chiral Manganese Complexes with Pinene Appended Tetradentate Ligands as Stereoselective Epoxidation Catalysts. *Dalton Trans.* **2007**, 5539−5545.
(21) Gómez, L.; Garcia-Bosch, I.; Company, A.; Benet-Buchholz, J.; Polo, A.; Sala, X.; Ribas, X.; Costas, M. Stereospecific C−H Oxidation with H_2O_2 Catalyzed by a Chemically Robust Site-Isolated Iron Catalyst. *Angew. Chem., Int. Ed.* **2009**, *48*, 5720−5723.
(22) Wu, M.; Wang, B.; Wang, S.; Xia, C.; Sun, W. Asymmetric Epoxidation of Olefins with Chiral Bioinspired Manganese Complexes. *Org. Lett.* **2009**, *11*, 3622−3625.
(23) Lyakin, O. Y.; Ottenbacher, R. V.; Bryliakov, K. P.; Talsi, E. P. Asymmetric Epoxidations with H_2O_2 on Fe and Mn Aminopyridine Catalysts: Probing the Nature of Active Species by Combined Electron Paramagnetic Resonance and Enantioselectivity Study. *ACS Catal.* **2012**, *2*, 1196−1202.
(24) Garcia-Bosch, I.; Ribas, X.; Costas, M. A Broad Substrate-Scope Method for Fast, Efficient and Selective Hydrogen Peroxide-Epoxidation. *Adv. Synth. Catal.* **2009**, *351*, 348−352.
(25) Vicens, L.; Olivo, G.; Costas, M. Remote Amino Acid Recognition Enables Effective Hydrogen Peroxide Activation at a Manganese Oxidation Catalys. *Angew. Chem., Int. Ed.* **2022**, *61*, No. e202114932.
(26) Ottenbacher, R. V.; Talsi, E. P.; Bryliakov, K. P. Chiral Manganese Aminopyridine Complexes: The Versatile Catalysts of Chemo- and Stereoselective Oxidations with H_2O_2. *Chem. Rec.* **2018**, *18*, 78−90.
(27) Cussó, O.; Garcia-Bosch, I.; Font, D.; Ribas, X.; Lloret-Fillol, J.; Costas, M. Highly Stereoselective Epoxidation with H_2O_2 Catalyzed by Electron-Rich Aminopyridine Manganese Catalysts. *Org. Lett.* **2013**, *15*, 6158−6161.
(28) Ottenbacher, R. V.; Samsonenko, D. G.; Talsi, E. P.; Bryliakov, K. P. Highly Enantioselective Bioinspired Epoxidation of Electron-Deficient Olefins with H2O2 on Aminopyridine Mn Catalysts. *ACS Catal.* **2014**, *4*, 1599−1606.
(29) Ottenbacher, R. V.; Samsonenko, D. G.; Talsi, E. P.; Bryliakov, K. P. Enantioselective Epoxidations of Olefins with Various Oxidants on Bioinspired Mn Complexes: Evidence for Different Mechanisms and Chiral Additive Amplification. *ACS Catal.* **2016**, *6*, 979−988.
(30) Cianfanelli, M.; Olivo, G.; Milan, M.; Klein Gebbink, R. J. M.; Ribas, X.; Bietti, M.; Costas, M. Enantioselective C-H Lactonization of Unactivated Methylenes Directed by Carboxylic Acids. *J. Am. Chem. Soc.* **2020**, *142*, 1584−1593.
(31) Ottenbacher, R. V.; Talsi, E. P.; Bryliakov, K. P. Mechanism of Selective C-H Hydroxylation Mediated by Manganese Aminopyridine Enzyme Models. *ACS Catal.* **2015**, *5*, 39−44.
(32) Shen, D.; Miao, C.; Xu, D.; Xia, C.; Sun, W. Highly Efficient Oxidation of Secondary Alcohols to Ketones Catalyzed by Manganese Complexes of N4 Ligands with H_2O_2. *Org. Lett.* **2015**, *17*, 54−57.
(33) Galeotti, M.; Vicens, L.; Salamone, M.; Costas, M.; Bietti, M. Resolving Oxygenation Pathways in Manganese-Catalyzed C(Sp^3)−H Functionalization via Radical and Cationic Intermediates. *J. Am. Chem. Soc.* **2022**, *144*, 7391−7401.
(34) Call, A.; Cianfanelli, M.; Besalú-Sala, P.; Olivo, G.; Palone, A.; Vicens, L.; Ribas, X.; Luis, J. M.; Bietti, M.; Costas, M. Carboxylic Acid Directed *γ*-Lactonization of Unactivated Primary C−H Bonds Catalyzed by Mn Complexes: Application to Stereoselective Natural Product Diversification. *J. Am. Chem. Soc.* **2022**, *144*, 19542−19558.
(35) Wegeberg, C.; Lauritsen, F. R.; Frandsen, C.; Mørup, S.; Browne, W. R.; McKenzie, C. J. Directing a Non-Heme Iron(III)-Hydroperoxide Species on a Trifurcated Reactivity Pathway. *Chem.—Eur. J.* **2018**, *24*, 5134−5145.
(36) Chen, J.; Draksharapu, A.; Angelone, D.; Unjaroen, D.; Padamati, S. K.; Hage, R.; Swart, M.; Duboc, C.; Browne, W. R. H2O2 Oxidation by FeIII-OOH Intermediates and Its Effect on Catalytic Efficiency. *ACS Catal.* **2018**, *8*, 9665−9674.
(37) Pijper, D.; Saisaha, P.; de Boer, J. W.; Hoen, R.; Smit, C.; Meetsma, A.; Hage, R.; van Summeren, R. P.; Alsters, P. L.; Feringa, B. L.; Browne, W. R.; Browne, W. R. The Unexpected Role of Pyridine-2-Carboxylic Acid in Manganese Based Oxidation Catalysis with Pyridin-2-yl Based Ligands. *Dalton Trans.* **2010**, *39*, 10375−10381.
(38) Groni, S.; Dorlet, P.; Blain, G.; Bourcier, S.; Guillot, R.; Anxolabéhère-Mallart, E. Reactivity of an Aminopyridine $[LMn^{II}]^{2+}$ Complex with H_2O_2. Detection of Intermediates at Low Temperature. *Inorg. Chem.* **2008**, *47*, 3166−3172.
(39) Oswald, V. F.; Weitz, A. C.; Biswas, S.; Ziller, J. W.; Hendrich, M. P.; Borovik, A. S. Manganese−Hydroxido Complexes Supported by a Urea/Phosphinic Amide Tripodal Ligand. *Inorg. Chem.* **2018**, *57*, 13341−13350.
(40) Biswas, S.; Mitra, A.; Banerjee, S.; Singh, R.; Das, A.; Paine, T. K.; Bandyopadhyay, P.; Paul, S.; Biswas, A. N. A High Spin Mn(IV)-Oxo Complex Generated via Stepwise Proton and Electron Transfer from Mn(III)−Hydroxo Precursor: Characterization and C−H Bond Cleavage Reactivity. *Inorg. Chem.* **2019**, *58*, 9713−9722.
(41) Yang, G.; Mikhalyova, E. A.; Filatov, A. S.; Kryatov, S. V.; Rybak-Akimova, E. V. Manganese(II) Complexes of 1,1′-Bis-[(Pyridin-2-yl)Methyl)]-2,2′-Bipiperidine (PYBP): Synthesis, Structure, Catalytic Properties in Alkene Epoxidation with Hydrogen Peroxide, and Related Mechanistic Studies. *Inorg. Chim. Acta* **2023**, *546*, 121288.
(42) Abdolahzadeh, S.; Boyle, N. M.; Hoogendijk, M. L.; Hage, R.; de Boer, J. W.; Browne, W. R.; Browne, W. R. The Role of Carboxylato Ligand Dissociation in the Oxidation of Chrysin with H_2O_2 Catalysed by $[Mn_2^{III,IV}(\mu\text{-}CH_3COO)(\mu\text{-}O)_2(Me_4Dtne)](PF_6)_2$. *Dalton Trans.* **2014**, *43*, 6322−6332.
(43) Baffert, C.; Collomb, M. N.; Deronzier, A.; Pécaut, J.; Limburg, J.; Crabtree, R. H.; Brudvig, G. W. Two New Terpyridine Dimanganese Complexes: A Manganese(III,III) Complex with a Single Unsupported Oxo Bridge and a Manganese(III,IV) Complex with a Dioxo Bridge. Synthesis, Structure, and Redox Properties. *Inorg. Chem.* **2002**, *41*, 1404−1411.
(44) Hureau, C.; Blondin, G.; Charlot, M. F.; Philouze, C.; Nierlich, M.; Césario, M.; Anxolabéhère-Mallart, E. Synthesis, Structure, and Characterization of New Mononuclear Mn(II) Complexes. Electrochemical Conversion into New Oxo-Bridged Mn_2(III,IV) Complexes. Role of Chloride Ions. *Inorg. Chem.* **2005**, *44*, 3669−3683.
(45) Collomb, M.-N.; Mantel, C.; Romain, S.; Duboc, C.; Leprêtre, J.-C.; Pécaut, J.; Deronzier, A. Redox-Induced *μ*-Acetato and *μ*-Oxo Core Interconversions in Dinuclear Manganese Tris(2-Methylpyridyl)Amine (TPA) Complexes: Isolation and Character-

https://doi.org/10.1021/acscatal.3c00866
ACS Catal. 2023, 13, 6403−6415

ization of $[Mn_2^{III}(\mu\text{-}O)(\mu\text{-}O_2CCH_3)(TPA)_2]^{3+}$. *Eur. J. Inorg. Chem.* **2007**, *2007*, 3179−3187.
(46) Berggren, G.; Thapper, A.; Huang, P.; Eriksson, L.; Styring, S.; Anderlund, M. F. Mechanistic Studies on the Water-Oxidizing Reaction of Homogeneous Manganese-Based Catalysts: Isolation and Characterization of a Suggested Catalytic Intermediate. *Inorg. Chem.* **2011**, *50*, 3425−3430.
(47) Wieghardt, K.; Bossek, U.; Ventur, D.; Weiss, J. Assembly and Structural Characterization of Binuclear M-Oxo-Di-μ-Acetato Bridged Complexes of Manganese(III). Analogues of the Di-Iron(III) Centre in Hemerythrin. *J. Chem. Soc. Chem. Commun.* **1985**, 347−349.
(48) Toftlund, H.; Markiewicz, A.; Murray, K. S.; Brekke, T.; Maartmann-Moe, K.; Tønnesen, H. H.; Tokii, T. Synthesis and Magnetic Properties of a mu-Oxo-Di(Mu-Acetato)Manganese(III) Complex of a Strapped Tripodal Pyridylamine Ligand N,N,N',N'-Tetrakis(2-Pyridylmethyl)-1,3-Propanediamine. A Model for the Mn_2 Site of Mn-Catalase Enzymes. *Acta Chem. Scand.* **1990**, *44*, 443−446.
(49) De Boer, J. W.; Browne, W. R.; Brinksma, J.; Alsters, P. L.; Hage, R.; Feringa, B. L. Mechanism of cis-Dihydroxylation and Epoxidation of Alkenes by Highly H_2O_2 Efficient Dinuclear Manganese Catalysts. *Inorg. Chem.* **2007**, *46*, 6353−6372.
(50) Chen, J.; Klein Gebbink, R. J. M. Deuterated N2Py2 Ligands: Building More Robust Non-Heme Iron Oxidation Catalysts. *ACS Catal.* **2019**, *9*, 3564−3575.
(51) Wang, B.; Lin, J.; Sun, Q.; Xia, C.; Sun, W. Efficient Aliphatic C-H Oxidation and C\C Epoxidation Catalyzed by Porous Organic Polymer-Supported Single-Site Manganese Catalysts. *ACS Catal.* **2021**, *11*, 10964−10973.
(52) Wang, B.; Lin, J.; Xia, C.; Sun, W. Porous Organic Polymer-Supported Manganese Catalysts with Tunable Wettability for Efficient Oxidation of Secondary Alcohols. *J. Catal.* **2022**, *406*, 87−95.

https://doi.org/10.1021/acscatal.3c00866
ACS Catal. 2023, 13, 6403−6415